



A voltammetric sensor for the detection of 2-aminophenol in the presence of bisphenol A using a carbon paste electrode modified with N-doped reduced graphene oxide/CuO nanocomposite and ionic liquid

Mostafa Poursoltani Zarandi¹ and Hadi Beitollahi^{2,*}

¹Department of Chemistry, Graduate University of Advanced Technology, Kerman, Iran

²Environment Department, Institute of Science and High Technology and Environmental Sciences, Graduate University of Advanced Technology, Kerman, Iran

Received: 5 March 2022

Accepted: 5 July 2022

Published online:

24 August 2022

© The Author(s), under exclusive licence to Springer Science+Business Media, LLC, part of Springer Nature 2022

ABSTRACT

In present work, a novel and facile electrode was constructed using the modification of carbon paste electrode (CPE) with N-doped reduced graphene oxide/CuO (N-rGO/CuO) and ionic liquid (IL) for electrochemically determination of 2-aminophenol. The N-rGO/CuO structure and morphology were investigated successfully employing Fourier transform infrared spectroscopy, energy-dispersive X-ray spectroscopy, field-emission scanning electron microscopy, and X-ray diffraction. Synergistic impact of N-rGO/CuO nanocomposite with IL could enhance electron transfer rate, highlighting greater catalytic activity of as-produced sensor towards the 2-aminophenol oxidation. According to results from differential pulse voltammetry (DPV), a linear relationship was found between peak currents and different 2-aminophenol concentrations in the range 0.1–700.0 μM , with small limit of detection (0.025 μM). In addition, the prepared sensor was used to determine 2-aminophenol and bisphenol A simultaneously via DPV. The N-rGO/CuO/ILCPE separates the oxidation peak potential of 2-aminophenol and bisphenol A by 320 mV. Furthermore, the sensor could excellently determine 2-aminophenol and bisphenol A in the water samples, and it showed a very high recovery percentage.

Address correspondence to E-mail: h.beitollahi@yahoo.com

1 Introduction

Environmental protection has become a concern around the world in recent years. The hazardous toxic environmental pollutants arising from industrial wastes and man-made activities threaten the lives of all living things [1]. One of such toxic pollutants is aromatic 2-amino phenols containing hydroxyl and amino groups on benzene ring, which have own benefits (such as amphoteric nature, good reducing agents, chemically reactive) and harms (such as easy dermal and cell membrane penetration leading to genotoxicity, mutagenicity and hepatotoxicity as well as deoxyribonucleic acid (DNA) damage induced by present metal ions) [2]. Harmful impacts are the results of extensive application of these compounds as raw materials in various industries, petroleum additives, chemical inhibitors and synthetic intermediates [3]. Accordingly, it is essential to determine the concentration of 2-aminophenol in various media using an effective analytical technique. Bisphenol A is a raw material extensively applied for the construction of epoxy resins and polycarbonate plastics, as well as thermal receipts, medical equipment, nursing bottles, canned beverage containers and pediatric toys. Limited amounts of bisphenol A can enter the human body by penetrating the packaging of food and beverage products [4–7]. This compound can disrupt the endocrine glands, thereby influencing the reproduction of aquatics and inducing various human health problems [8]. Accordingly, it is vital to develop an effective method to rapidly and sensitively determine the concentration of bisphenol A in various media. In this regard, there have been various analytical techniques to detect the presence of highly toxic and low degradable bisphenol A and 2-aminophenol, including spectrophotometry [9], chromatography [10], and also electrochemical approaches [11, 12].

It should be mentioned that the electrochemical methods have been special in this context owing to merits like inexpensiveness, rapid response, facile facilities and easy to use [13–22]. Electrochemical sensing is continuously growing area in the electrochemical fields. When comparing with conventional electrodes, chemically modified electrodes (CMEs) have impressive reduction/oxidation potential, rapid kinetics of electron transfer, admirable electro-optical properties and stable electrode surfaces in electroanalysis [23–32]. Nanotechnology has led to great

advances in various fields [33–35]. Nanomaterials provided promising ground for the development of various potent analytical approaches like electrochemical sensors for sensitively and selectivity monitoring [36–42].

Graphene is a two-dimensional monolayer of sp^2 -hybridized carbon atoms spiked in a honeycomb lattice, which attracted further attention of many investigations owing to features like excellent electronic conductivity, affordability, and superior mechanical and chemical stability [43]. These are probably due to interlayer distance, specific surface area, doping and porous nature. In this regard, there are numerous advances including graphene foam formation [44], template-assisted assembly [45], graphene and carbon nanotube recombination [46] and heteroatom integration with graphene [47]. Among these, the electrochemical sensing activity of graphene-based electrodes has been reinforced following nitrogen (N) doping [48, 49], probably due to induction of more active sites via doping, and enlargement of specific surface area. Reduced graphene oxide (rGO)-anchored semiconductors exhibited greater catalytic performance when comparing with other materials [50, 51]. The copper oxide (CuO) as an intrinsically p-type semi-conductor, with a band gap of about 1.2 eV, excellent electrocatalytic and electrochemical properties and high availability, has been widely applied to fabricate electrochemical sensors [52–54].

Ionic liquids (ILs) are organic compounds that composed of organic cations with different anions, which are often found as liquid at ambient temperature. They have been extensively applied in electrochemical sensors because of specific physicochemical properties, some of which are fairly great ionic conductivity, poor vapor pressure, admirable chemical stability, impressive biocompatibility and stable electrochemical windows [55, 56].

Therefore, in this work, the CuO/N-rGO nanocomposite and IL modified CPE was used as electrochemical sensor to detect 2-aminophenol. A series of electrochemical tests like differential pulse voltammetry (DPV), cyclic voltammetry (CV), and chronoamperometry (CHA) have shown that N-rGO/CuO/ILCPE exhibited better electrochemical performance for 2-aminophenol through the synergistic effects of prepared N-rGO/CuO nanocomposite and IL. In addition, we investigated the performance of the N-rGO/CuO/ILCPE for

simultaneous detection of 2-aminophenol and bisphenol A. Moreover, to evaluate the developed electrode, the identification of 2-aminophenol and bisphenol A in the real specimens was performed and the obtained results were satisfying.

2 Experimental section

2.1 Apparatus and chemicals

PGSTAT-302 N Autolab potentiostat/galvanostat (Eco Chemie, Netherlands) was a device to perform all electrochemical tests whose data were analyzed by General Purpose Electrochemical System (GPES) software. The electrochemical tests were performed in an electrochemical cell with three-electrode setup, containing N-rGO/CuO/ILCPE (working electrode (WR)), a platinum wire (counter electrode (CE)), and an Ag/AgCl (3.0 M KCl) (reference electrode (RE)). The pH values were measured by a digital pH meter (Metrohm type 713) equipped with a combined glass electrode in all solutions. Panalytical X'Pert Pro X-ray diffractometer equipped with Cu/K α radiation ($\lambda = 1.5418$ nm) was employed to obtain X-ray diffraction (XRD) spectra to characterize the nanoparticles for crystal structures. Field emission-scanning electron microscopy FE-SEM images (MIRA3 scanning electron microscope; Tescan, Czech Republic) were analyzed to explore the N-rGO/CuO morphology. The as-fabricated products were examined for the chemical compositions using EDX plus FE-SEM. Bruker Tensor II spectrometer (Germany) was used to record the FT-IR patterns.

All materials used in this work had analytical grade. GO and Cu(II) acetate were bought from Sigma-Aldrich (Germany). 2-aminophenol, bisphenol A and other chemicals were bought from the Merck (Germany).

2.2 Preparation of N-rGO/CuO nanocomposite

In a facile preparation process of N-rGO/CuO nanocomposite, the GO (20 mg) was dissolved in deionized water (20 ml) under ultrasonic conditions, which results in the production of clear suspension. Then, the suspension was appended with 1.6 g of copper(II) acetate (Cu(OAc) $_2$) while stirring vigorously for 50 min, followed by adding NH $_3$ ·H $_2$ O (wt

25%) as dropwise while stirring continuously. The obtained mixture was placed in a Teflon Lined autoclave at a temperature of 180 °C for 12 h, followed by cooling down at an ambient temperature, washing with distilled water for several times. The result was N-rGO/CuO nanocomposite that was dried in an oven at 60 °C for 12 h.

2.3 Preparation of N-rGO/CuO/ILCPE

The N-rGO/CuO/ILCPE was prepared by grounding N-rGO/CuO nanocomposite and graphite powder (10:90 wt/wt%), followed by hand mixing with paraffin oil and IL (1-butyl-3-methylimidazolium hexafluorophosphate) (70:30 v/v%) in a mortar and pestle for at least 40 min until a homogenous wetted paste was obtained. The modified electrode was assembled by tightly pressing the resulting paste in the end-cavity of a substrate (glass tube). Then, the electrical contact was made by a Cu wire. Before each test, the surface of modified CPE was refreshed by pushing out a small portion of prepared paste and polishing it on a soft paper.

3 Results and discussion

3.1 Characterizations of the N-rGO/CuO nanocomposite

The FT-IR spectra of the GO and N-rGO/CuO nanocomposite is presented in Fig. 1. In the characteristic spectrum of GO, various functional groups in the structure include the vibration modes of O–H (3428 cm $^{-1}$), C=C (1577 cm $^{-1}$), C=O (1720 cm $^{-1}$)

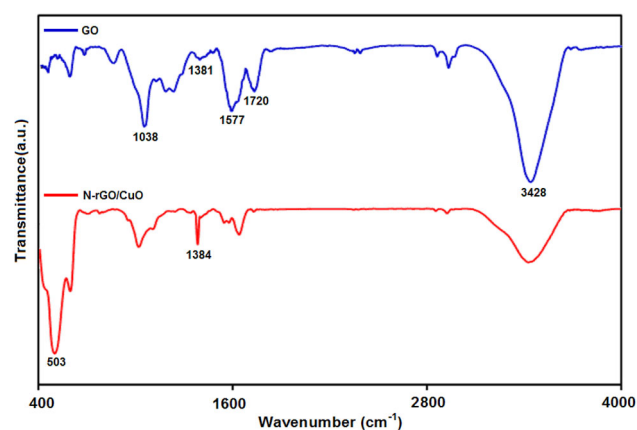


Fig. 1 FT-IR spectrum of GO, and N-rGO/CuO nanocomposite

and epoxy C–O–C (1038 cm^{-1}) and phenolic C–O (1381 cm^{-1}). The characteristic peaks were related to a plenty of oxygen groups like carbonyl, carboxyl and hydroxyl groups on the GO surface. In the spectrum of N-rGO/CuO nanocomposite, the decline in the intensity of the characteristic bands in GO emphasized the reduction of GO into rGO. Moreover, the peak of absorption at 503 cm^{-1} attributed to Cu–O stretching vibrations which emphasized that CuO was decorated on rGO sheets. The doping of N is further indicated by the appearance of a new peak in the vicinity of 1384 cm^{-1} , which was due to C–N stretching.

The morphology of as prepared N-rGO/CuO nanocomposites was analyzed by FE-SEM (Fig. 2). It is clearly can be seen in Fig. 2, the planar sheets of rGO with waved and wrinkled surface due to the nitrogen doping in rGO. Furthermore, the CuO NPs with an almost spherical morphology and a diameter between of 15 and 50 nm are homogeneously distributed on the surface of the N-rGO.

The EDX cleared the elemental or chemical formula of the synthesized N-rGO/CuO nanocomposite (Fig. 3), the results of which verified the existence of elements (C, N, Cu and O) in N-rGO/CuO nanocomposite.

The phase structure of N-rGO/CuO was identified by XRD. The XRD diffraction peaks of GO and N-

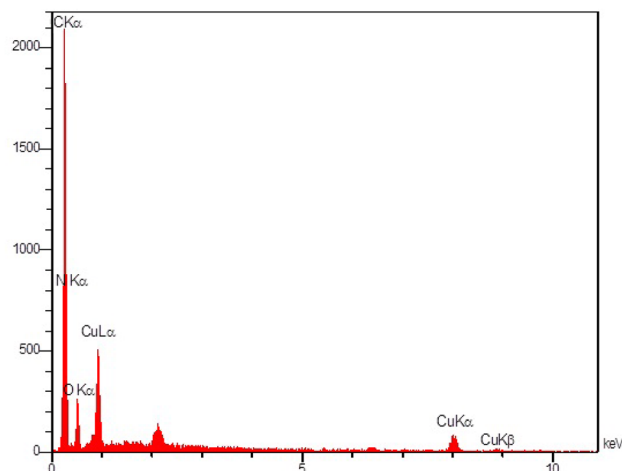


Fig. 3 The EDX spectrum of N-rGO/CuO nanocomposite

rGO/CuO are shown in Fig. 4. GO displayed a diffraction peak (001) at 11.5° and a small peak (101) at 42.8° . The peaks at $2\theta = 32.49^\circ, 35.54^\circ, 38.76^\circ, 48.77^\circ, 53.72^\circ, 58.23^\circ, 61.58^\circ, 66.22^\circ, 68.06^\circ, 72.40^\circ,$ and 75.187° as shown in Fig. 4 (N-rGO/CuO nanocomposite) corresponded to the planes (-110), (002), (111), (-202), (020), (202), (-113), (-311), (-220), (311) and (-222) related to CuO (JCPDS 00-045-0937), respectively. Considering these results, the CuO crystallization and nuclearization are evident within production. No peak of GO diffraction confirmed the GO reduction within hydrothermal reaction. No peak

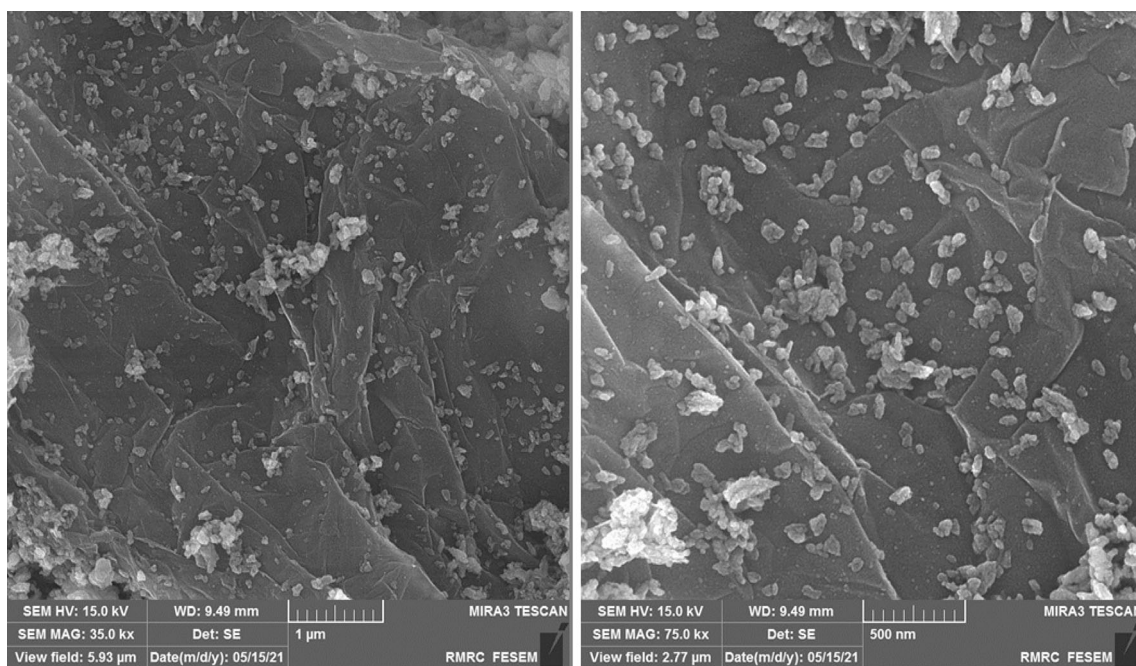


Fig. 2 FE-SEM images of N-rGO/CuO nanocomposite at different magnifications

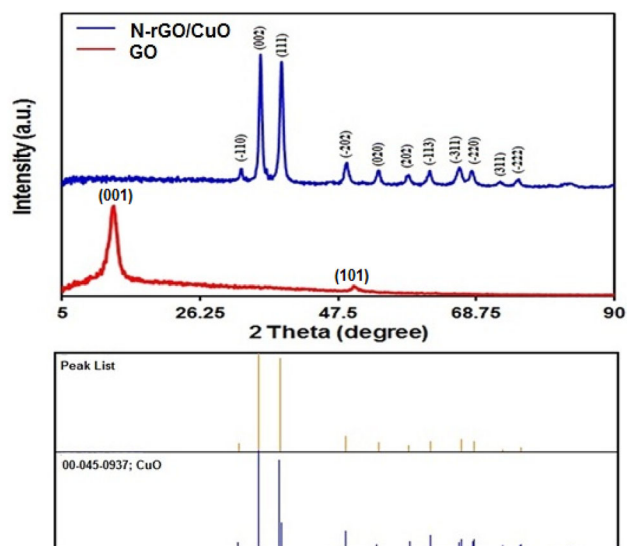


Fig. 4 XRD pattern of GO and N-rGO/CuO nanocomposite

of graphene diffraction highlighted rGO rare restacking. Potent interfacial bonding of CuO NPs with N-rGO surface possessed a positive impact on preventing rGO restacking and preserving N-rGO structure [57]. The crystallite size (D) of CuO nanoparticles have been calculated from XRD by Debye Sheerer Equation:

$$D = K\lambda/\beta \cos \theta.$$

It was found that the average crystallite size of the CuO nanoparticles was determined by XRD spectrum about 17.7 nm.

3.2 Electrochemical behavior of 2-aminophenol at the N-rGO/CuO/ILCPE

The DPV method was recruited to study the effect pH value of electrolyte solution (0.1 M PBS) in different pH values (2–9) in the presence of 200.0 μM of 2-aminophenol on the N-rGO/CuO/ILCPE surface. The best catalytic performance occurred at pH 7. Therefore, pH 7 was selected as the optimum pH in the 2-aminophenol detection.

Figure 5 display CVs of electrochemical oxidation of 200.0 μM of 2-aminophenol on the bare CPE (curve a), N-rGO/CuO/CPE (curve b), ILCPE (curve c) and N-rGO/CuO/ILCPE (curve d). In accordance with results (Fig. 5), the 2-aminophenol oxidation was very poor on the bare CPE surface. However, at the surface of the N-rGO/CuO/ILCPE, the oxidation peak of 2-aminophenol occurred at lower potentials

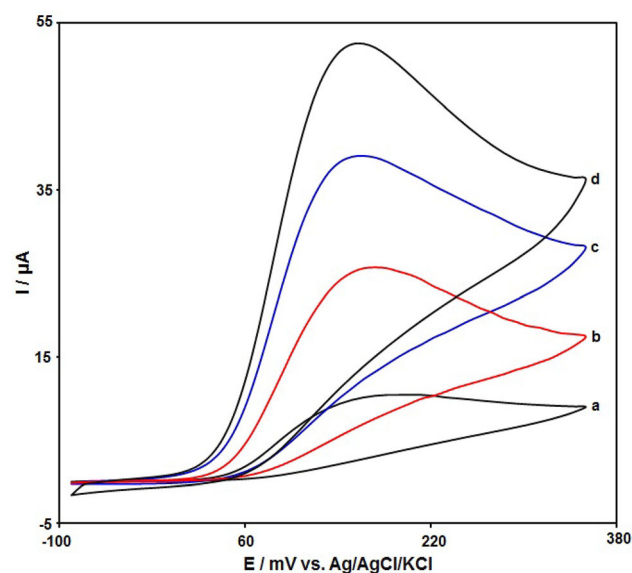


Fig. 5 CVs of 200.0 μM 2-aminophenol at (a) bare CPE, (b) N-rGO/CuO/CPE, (c) ILCPE and (d) N-rGO/CuO/ILCPE in 0.1 M PBS of pH 7.0

and had a higher anodic current compared to other CPEs. This result is probably due to synergistic impact of N-rGO/CuO nanocomposite and IL.

3.3 Effect of the scan rate (v) on the results

The CV method was used to explore the influence of scan rate on the oxidation of 2-aminophenol (400.0 μM) in 0.1 M PBS, as shown in Fig. 6. An elevation in the scan rate (10–600 mV/s) enhanced the oxidation peak current of 2-aminophenol, in addition to gradually shifting the anodic potentials to more positive values. Figure 6 (inset) emphasizes the proportionality of the anodic response current linearly to the scan rate square root, which shows controlled-diffusion processes for the electrocatalytic oxidation of 2-aminophenol on N-rGO/CuO /ILCPE.

3.4 Chronoamperometric analyse

Chronoamperometry was considered for the investigation of 2-aminophenol electro-oxidation at the potential of 210 mV and various analyte concentrations in 0.1 M PBS (pH 7.0), as seen in Fig. 7. The current response of electroactive 2-aminophenol was described under a diffusion-limited electrocatalytic process using Cottrell's equation [58]:

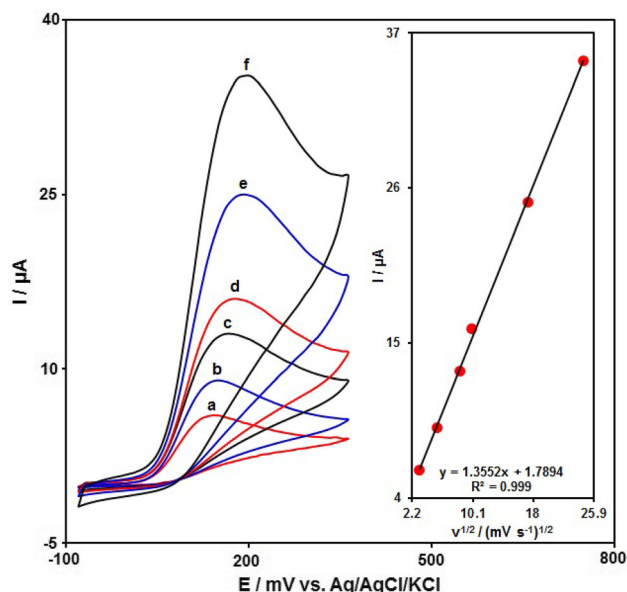


Fig. 6 Cyclic voltammetric responses of 400.0 μM 2-aminophenol in 0.1 M PBS (pH 7.0) at various scan rates (a: 10, b: 30, c: 70, d: 100, e: 300, and f: 600 mV/s) at N-rGO/CuO/ILCPE. Inset: Plot of the square root of the scan rate vs. the oxidation peak currents of 2-aminophenol

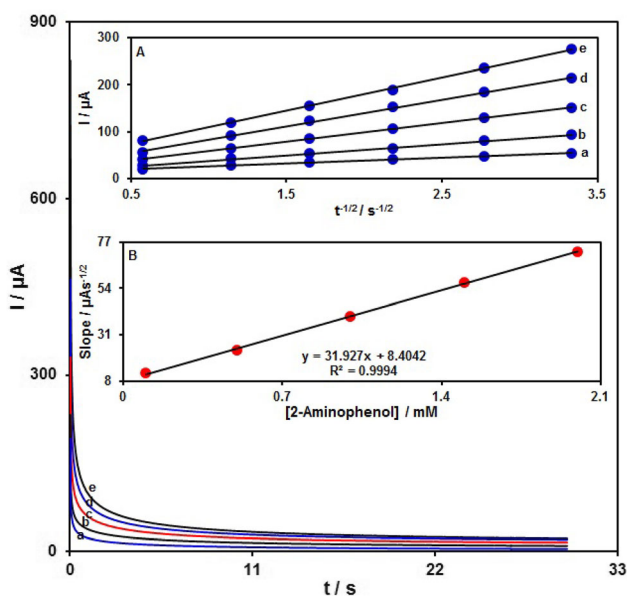


Fig. 7 The chronoamperograms obtained at N-rGO/CuO/ILCPE in 0.1 M PBS at pH of 7.0 for different concentrations of 2-aminophenol (a: 0.1, b: 0.5, c: 1.0, d: 1.5, and e: 2.0 mM of 2-aminophenol). Insets (A): plots of I against $t^{-1/2}$ (from chronoamperograms for the 2-aminophenol content of 0.1–2.0 mM); (B) plot of slope from straight lines against various 2-aminophenol contents

$$I = nFAD^{1/2}C_b\pi^{-1/2}t^{-1/2}.$$

In this equation, n stands for the number of electron transfer exchanged per reactant molecule, F for the Faraday constant, C_b for 2-aminophenol concentration (mol/cm^3), and D for diffusion coefficient (cm^2/s). The plot of I versus $t^{-1/2}$ provided various linear curves for different 2-aminophenol contents of 0.1–2.0 mM (Fig. 7, inset A). The slope of each straight line against the 2-aminophenol content eventually made it possible to calculate the overall slope of the best-fit line (Fig. 7, inset B). At last, the overall slope in the Cottrell's equation was utilized to estimate the mean D value, which was $4.2 \times 10^{-5} \text{ cm}^2/\text{s}$.

3.5 Calibration curve

The calibration curve for 2-aminophenol detection was achieved by DPVs for the oxidation of various 2-aminophenol concentrations in PBS (0.1 M, pH 7.0). Figure 8 illustrates the DPVs for the N-rGO/CuO/ILCPE toward various 2-aminophenol concentrations. Based on Fig. 8(inset), there was a linear elevation in the peak currents of 2-aminophenol

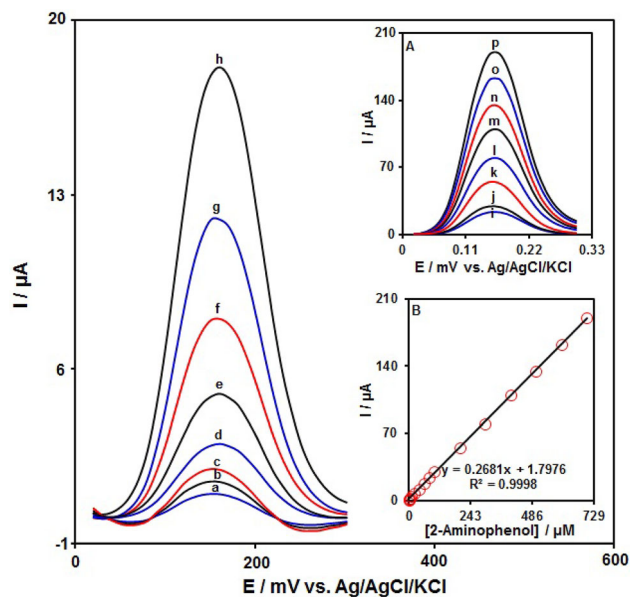


Fig. 8 DPV response of 2-aminophenol at N-rGO/CuO/ILCPE in the concentration range 0.1–60.0 μM in 0.1 M PBS of pH 7.0 (a–h refers to 0.1, 0.5, 1.0, 5.0, 10.0, 20.0, 40.0, and 60.0 μM). Insets: A DPV response of 2-aminophenol in the concentration range 80.0–700.0 μM (i–p refers to 80.0, 100.0, 200.0, 300.0, 400.0, 500.0, 600.0, and 800.0 μM); B The calibration curve of DPV peaks against [2-aminophenol]

oxidation by increasing its concentration. The results revealed the linear dynamic range from 0.1 μM to 700.0 μM, with a narrow limit of detection (LOD, $S/N = 3$) of 0.025 μM. Moreover, the Table 1 presented that the N-rGO/CuO/ILCPE was successfully used to determinate 2-aminophenol comparing with other sensors.

3.6 Detection of 2-aminophenol and bisphenol A simultaneously on N-rGO/CuO/ILCPE

The DPVs for detection of 2-aminophenol and bisphenol A simultaneously via N-rGO/CuO/ILCPE are shown in Fig. 9. The peaks at 160 and 480 V were related to the oxidation of 2-aminophenol and bisphenol A, respectively. The voltammetric peak currents of these analytes increased linearly with increasing their concentrations. Figure 9(inset A and inset B) show the corresponding calibration curves for 2-aminophenol and bisphenol A, respectively. The slope of 2-aminophenol calibration curve (0.2675 μA/μM) was almost equal to that without bisphenol A (0.2681 μA/μM, see previous section), indicating the applicability of N-rGO/CuO/ILCPE for detection the concentrations of 2-aminophenol in the presence of bisphenol A.

3.7 Interference study

The influence of numerous substances on the determination of 2-aminophenol was investigated in 0.1 M PBS (pH 7.0) containing 30.0 μM 2-aminophenol in the presence of possible interfering substances. The

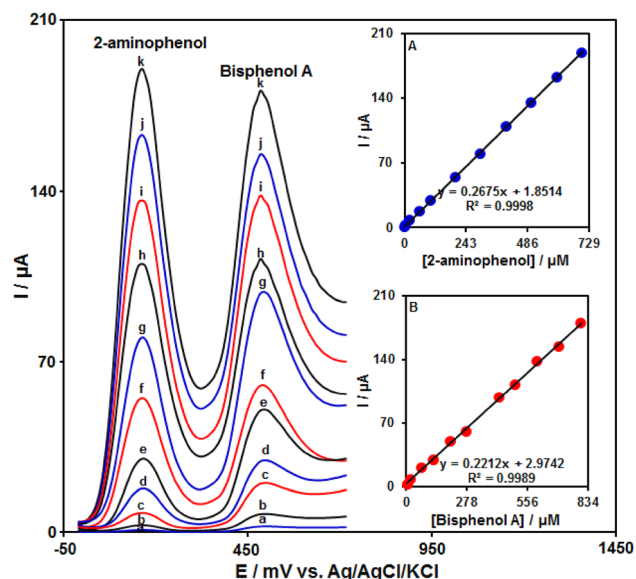


Fig. 9 The DPVs of the N-rGO/CuO/ILCPE in 0.1 M PBS at pH equal to 7.0 containing different concentrations of 2-aminophenol and bisphenol A. Notably, a–k corresponded to 0.1 + 0.1, 5.0 + 5.0, 20.0 + 20.0, 60.0 + 60.0, 100.0 + 100.0, 200.0 + 200.0, 300.0 + 300.0, 400.0 + 400.0, 500.0 + 500.0, 600.0 + 600.0 and 700.0 + 700.0 μM of 2-aminophenol and bisphenol A, respectively. Inset **A** The I_p plot vs. 2-aminophenol concentration. Inset **B** The I_p plot vs. bisphenol A concentration

results show that 600-fold K^+ , Ca^{2+} , Mg^{2+} , Al^{3+} , NH_4^+ , Cl^- , Br^- and SO_4^{2-} , 25-fold phenol, P-nitrophenol, O-nitrophenol and O-phenylenediamine, 10-fold hydroquinone, catechol, and resorcinol did not show any significant change in the peak current of 2-aminophenol. These results demonstrated that the N-rGO/CuO/ILCPE provides a selective sensor toward the determination of 2-aminophenol.

Table 1 A comparison between the obtained linear range and limit of detection of 2-aminophenol sensor in the present work and the other reported works

Electrochemical sensor	Method	Linear dynamic range	Limit of detection (μM)	References
Multi-walled carbon nano-tube-cobalt tetra substituted sorbaamide phthalocyanine/glassy carbon electrode	DPV	0.1–38 μM	0.03	[59]
Amino-functionalized SBA-15 mesoporous silica/CPE	DPV	0.3–18 μM	0.05	[60]
Gold nanoparticles-reduced graphene oxide/glassy carbon electrode	DPV	0.4–50 μM	0.056	[61]
Zirconosilicate/CPE	DPV	120 nM to 500 μM	30.0	[62]
Single-wall carbon nanotubes-poly(4-aminopyridine)/glassy carbon electrode	Voltammetry	0.2–100 μM	40	[63]
N-rGO/CuO/ILCPE	DPV	0.1–700.0 μM	0.025	This work

Table 2 Applicability of N-rGO/CuO/ILCPE for sensing different concentrations (μM) of 2-aminophenol and bisphenol A spiked in real specimens ($n = 5$)

Sample	Spiked		Found		Recovery (%)		R.S.D. (%)	
	2-Aminophenol	Bisphenol A	2-Aminophenol	Bisphenol A	2-Aminophenol	Bisphenol A	2-Aminophenol	Bisphenol A
Tap water	0	0	–	–	–	–	–	–
	5.0	4.5	5.1	4.4	102.0	97.8	2.4	2.9
	6.0	5.5	5.9	5.7	98.3	103.6	2.2	3.1
	7.0	6.5	7.1	6.3	101.4	96.9	3.4	1.8
	8.0	7.5	7.9	7.6	98.7	101.3	1.7	2.5
River water	0	0	–	–	–	–	–	–
	4.0	6.5	3.9	6.5	97.5	101.5	3.6	1.9
	6.0	7.5	6.1	7.3	101.7	97.3	2.1	3.2
	8.0	8.5	8.2	8.4	102.5	98.8	2.7	2.4
	10.0	9.5	9.9	9.7	99.0	102.1	1.8	2.1

3.8 Analytical application

The 2-aminophenol and bisphenol A detection in the water samples was performed using N-rGO/CuO/ILCPE sensor. The determination of these analytes was carried out according to the standard addition method for five times in each concentration. Attained findings are summarized in Table 2, the recovery is between 96.9 and 103.6%, and the relative standard deviations (RSDs) are all less than or equal to 3.6%. According to Table 2, the acceptable results confirm good performance ability of N-rGO/CuO/ILCPE for the determination of 2-aminophenol and bisphenol A in water samples.

4 Conclusions

In this work, the N-rGO/CuO nanocomposite was synthesized through a simple hydrothermal method and characterized by various techniques, for example, FT-IR, FE-SEM, EDX, and XRD. Then, the prepared N-rGO/CuO/ILCPE was successfully used for 2-aminophenol detection. The proposed sensor displayed excellent electrocatalytic activity toward the electrochemical detection of 2-aminophenol by reducing the overvoltage and increasing the signal. The linear calibration curve was seen by drawing a plot of peak currents versus different 2-aminophenol levels (0.1–700.0 μM), presenting a low limit of

detection (0.025 μM). Two clear and well-separated voltammetric peaks along with the remarkably increased electro-oxidation currents of 2-aminophenol and bisphenol A were obtained on the modified electrode (N-rGO/CuO/ILCPE) in DPV measurements. Furthermore, the concentration of 2-aminophenol and bisphenol A were assayed in water samples, the recoveries were from 96.9 to 103.6%.

Author contribution

All authors participated in the analysis, writing and revising the manuscript.

Data availability

Materials described in the manuscript, including all relevant raw data, will be freely available to any researcher wishing to use them for non-commercial purposes, without breaching participant confidentiality

Declarations

The authors have no conflicts of interest.

Conflict of interest The authors have no Competing Interests.

References

1. M.M. Rahmana, M.M. Alam, A.M. Asiri, M.A. Islam, 3,4-Diaminotoluene sensor development based on hydrothermally prepared MnCoxOy nanoparticles. *Talanta* **176**, 17–25 (2018)
2. Y. Ohkuma, S. Kawanishi, Oxidative DNA damage induced by a metabolite of carcinogenic o-anisidine: enhancement of DNA damage and alteration in its sequence specificity by superoxide dismutase. *Arch. Biochem. Biophys.* **389**, 49–56 (2001)
3. E.A. Zeid, A.M. Nassar, M.A. Hussein, M.M. Alam, A.M. Asiri, H.H. Hegazy, M.M. Rahman, Mixed oxides CuO-NiO fabricated for selective detection of 2-Aminophenol by electrochemical approach. *J. Mater. Res. Technol.* **9**, 1457–1467 (2020)
4. W. Guo, A. Zhang, X. Zhang, C. Huang, D. Yang, N. Jia, Multiwalled carbon nanotubes/gold nanocomposites-based electrochemiluminescent sensor for sensitive determination of bisphenol A. *Anal. Bioanal. Chem.* **408**, 7173–7180 (2016)
5. A. Ghanam, A.A. Lahcen, A. Amine, Electroanalytical determination of Bisphenol A: Investigation of electrode surface fouling using various carbon materials. *J. Electroanal. Chem.* **789**, 58–66 (2017)
6. G.F. Pereira, L.S. Andrade, R.C. Rocha-Filho, N. Bocchi, S.R. Biaggio, Electrochemical determination of Bisphenol A using a boron-doped diamond electrode. *Electrochim. Acta* **82**, 3–8 (2012)
7. C. Hou, W. Tang, C. Zhang, Y. Wang, N. Zhu, A novel and sensitive electrochemical sensor for Bisphenol A determination based on carbon black supporting ferrocene oxide nanoparticles. *Electrochim. Acta* **144**, 324–331 (2014)
8. K. Deng, X. Liu, C. Li, Z. Hou, H. Huang, A comparative study of different Fe₃O₄-functionalized carbon-based nanomaterials for the development of electrochemical sensors for Bisphenol A. *Anal. Methods* **9**, 5509–5517 (2017)
9. R. Zhang, L. Zhao, R. Liu, Deciphering the toxicity of Bisphenol a to candida rugosa lipase through spectrophotometric methods. *J. Photochem. Photobiol. B: Biol.* **163**, 40–46 (2016)
10. L. Ren, J. Fang, G. Liu, J. Zhang, Z. Zhu, H. Liu, S. Lu, Simultaneous determination of urinary parabens, bisphenol A, triclosan, and 8-hydroxy-2'-deoxyguanosine by liquid chromatography coupled with electrospray ionization tandem mass spectrometry. *Anal. Bioanal. Chem.* **408**, 2621–2629 (2016)
11. K. Reddaiah, T.M. Reddy, Electrochemical biosensor based on silica sol-gel entrapment of horseradish peroxidase onto the carbon paste electrode toward the determination of 2-aminophenol in non-aqueous solvents: a voltammetric study. *J. Mol. Liq.* **196**, 77–85 (2014)
12. M. Kim, Y.E. Song, J.Q. Xiong, K.Y. Kim, M. Jang, B.H. Jeon, J.R. Kim, Electrochemical detection and simultaneous removal of endocrine disruptor, bisphenol A using a carbon felt electrode. *J. Electroanal. Chem.* **880**, 114907 (2021)
13. J. Mohanraj, D. Durgalakshmi, R.A. Rakkesh, S. Balakumar, S. Rajendran, H. Karimi-Maleh, Facile synthesis of paper based graphene electrodes for point of care devices: A double stranded DNA (dsDNA) biosensor. *J. Colloid Interface Sci.* **566**, 463–472 (2020)
14. M. Montazarolmahdi, M. Masrournia, A. Nezhadali, A new electrochemical approach for the determination of phenylhydrazine in water and wastewater samples using amplified carbon paste electrode. *Chem. Methodol.* **4**, 732–742 (2020)
15. Y. Pei, M. Hu, Y. Xia, W. Huang, Z. Li, S. Chen, Electrochemical preparation of Pt nanoparticles modified nanoporous gold electrode with highly rough surface for efficient determination of hydrazine. *Sens. Actuators B: Chem.* **304**, 127416 (2020)
16. S. Tajik, H. Beitollahi, M.B. Askari, A. Di Bartolomeo, Screen-printed electrode surface modification with NiCo₂O₄/RGO nanocomposite for hydroxylamine detection. *Nanomaterials* **11**, 3208 (2021)
17. H. Karimi-Maleh, F. Karimi, Y. Orooji, G. Mansouri, A. Razmjou, A. Aygun, F. Sen, A new nickel-based co-crystal complex electrocatalyst amplified by NiO dope Pt nanostructure hybrid; a highly sensitive approach for determination of cysteamine in the presence of serotonin. *Sci. Rep.* **10**, 1–13 (2020)
18. M. Payehghadr, Y. Taherkhani, A. Maleki, F. Nourifard, Selective and sensitive voltammetric sensor for methocarbamol determination by molecularly imprinted polymer modified carbon paste electrode. *Eurasian Chem. Commun.* **2**, 982–990 (2020)
19. S. Tajik, H. Beitollahi, F. Garkani-Nejad, M. Safaei, P. Mohammadzadeh-Jahani, Electrochemical sensing of Sudan I using the modified graphite screen-printed electrode. *Int. J. Environ. Anal. Chem.* (2020). <https://doi.org/10.1080/03067319.2020.1738418>
20. T. Eren, N. Atar, M.L. Yola, H. Karimi-Maleh, A sensitive molecularly imprinted polymer based quartz crystal microbalance nanosensor for selective determination of lovastatin in red yeast rice. *Food Chem.* **185**, 430–436 (2015)
21. S. Tajik, H. Beitollahi, Z. Dourandish, K. Zhang, Q.V. Le, T.P. Nguyen, S.Y. Kim, M. Shokouhimehr, Recent advances in the electrochemical sensing of venlafaxine: an antidepressant drug and environmental contaminant. *Sensors* **20**, 3675 (2020)
22. H. Karimi-Maleh, M. Sheikhshoaie, I. Sheikhshoaie, M. Ranjbar, J. Alizadeh, N.W. Maxakato, A. Abbaspourrad, A novel electrochemical epinine sensor using amplified CuO

- nanoparticles and an-hexyl-3-methylimidazolium hexafluorophosphate electrode. *New J. Chem.* **43**, 2362–2367 (2019)
23. M. Shahsavari, S. Tajik, I. Sheikhshoae, F. Garkani-Nejad, H. Beitollahi, Synthesis of Fe₃O₄@copper (II) imidazolate nanoparticles: Catalytic activity of modified graphite screen printed electrode for the determination of levodopa in presence of melatonin. *Microchem J.* **170**, 106637 (2021)
 24. M. Shivakumar, M.S. Dharmaprakash, S. Manjappa, K.L. Nagashree, Green synthesis of silver nanoparticles (SNPs)-modified electrode for electrochemical detection of nitrobenzene. *J. Iran. Chem Soc* **17**, 893–900 (2020)
 25. H. Sadeghi, S. Shahidi, S. Naghizadeh Raesi, A. Ghorbani-HasanSaraei, F. Karimi, Electrochemical determination of folic acid in fruit juices samples using electroanalytical sensor amplified with CuO/SWCNTs and 1-Butyl-2,3-dimethylimidazolium Hexafluorophosphate. *Chem. Methodol.* **4**, 743–753 (2020)
 26. H. Beitollahi, S. Tajik, H. Parvan, H. Soltani, A. Akbari, M.H. Asadi, Nanostructured based electrochemical sensor for voltammetric determination of ascorbic acid in pharmaceutical and biological samples. *Anal. Bioanal Electrochem.* **6**, 54–66 (2014)
 27. H. Karimi-Maleh, R. Darabi, M. Shabani-Nooshabadi, M. Baghayeri, F. Karimi, J. Rouhi, C. Karaman, Determination of D&C Red 33 and Patent Blue V Azo dyes using an impressive electrochemical sensor based on carbon paste electrode modified with ZIF-8/g-C₃N₄/Co and ionic liquid in mouthwash and toothpaste as real samples. *Food Chem. Toxicol.* **162**, 112907 (2022)
 28. H. Beitollahi, S. Tajik, M.H. Asadi, P. Biparva, Application of a modified graphene nanosheet paste electrode for voltammetric determination of methyl dopa in urine and pharmaceutical formulation. *J. Anal. Sci. Technol.* **5**, 1–9 (2014)
 29. S.S. Moshirian-Farahi, H.A. Zamani, M. Abedi, Nano-molar level determination of isoprenaline in pharmaceutical and clinical samples; A nanostructure electroanalytical strategy. *Eurasian Chem. Commun.* **2**, 702–711 (2020)
 30. H. Karimi-Maleh, A. Khataee, F. Karimi, M. Baghayeri, L. Fu, J. Rouhi, R. Boukherroub, A green and sensitive guanine-based DNA biosensor for idarubicin anticancer monitoring in biological samples: a simple and fast strategy for control of health quality in chemotherapy procedure confirmed by docking investigation. *Chemosphere* **291**, 132928 (2022)
 31. F. Garkani-Nejad, H. Beitollahi, S. Tajik, S. Jahani, La³⁺-doped Co₃O₄ nanoflowers modified graphite screen printed electrode for electrochemical sensing of vitamin B₆. *Anal. Bioanal Chem. Res.* **6**, 69–79 (2019)
 32. S.A. Alavi-Tabari, M.A. Khalilzadeh, H. Karimi-Maleh, Simultaneous determination of doxorubicin and dasatinib as two breast anticancer drugs uses an amplified sensor with ionic liquid and ZnO nanoparticle. *J. Electroanal. Chem.* **811**, 84–88 (2018)
 33. K.G. Shevchenko, I.S. Garkushina, F. Canfarotta, S.A. Piletsky, N.A. Barlev, Nano-molecularly imprinted polymers (nanoMIPs) as a novel approach to targeted drug delivery in nanomedicine. *RSC Adv.* **12**, 3957–3968 (2022)
 34. H. Karimi-Maleh, C. Karaman, O. Karaman, F. Karimi, Y. Vasseghian, L. Fu, A. Mirabi, Nanochemistry approach for the fabrication of Fe and N co-decorated biomass-derived activated carbon frameworks: a promising oxygen reduction reaction electrocatalyst in neutral media. *J. Nanostruct. Chem.* (2022). <https://doi.org/10.1007/s40097-022-00492-3>
 35. I. Amar, A. Sharif, M. Ali, S. Alshareef, F. Altohami, M. Abdulqadir, M. Ahwidi, Removal of methylene blue from aqueous solutions using nano-magnetic adsorbent based on zinc-doped cobalt ferrite. *Chem. Methodol.* **4**, 1–18 (2020)
 36. H. Karimi-Maleh, A.F. Shojaei, K. Tabatabaieian, F. Karimi, S. Shakeri, R. Moradi, Simultaneous determination of 6-mercaptopruine, 6-thioguanine and dasatinib as three important anticancer drugs using nanostructure voltammetric sensor employing Pt/MWCNTs and 1-butyl-3-methylimidazolium hexafluorophosphate. *Biosens. Bioelectron.* **86**, 879–884 (2016)
 37. H. Beitollahi, M. Mazloum Ardakani, H. Naeimi, B. Ganjipour, Electrochemical characterization of 2,2'-[1,2-ethanediylbis (nitriolethylidene)]-bis-hydroquinone-carbon nanotube paste electrode and its application to simultaneous voltammetric determination of ascorbic acid and uric acid. *J. Solid State Electrochem.* **13**, 353–363 (2009)
 38. A. Hosseini Fakhrrabad, R. Sanavi Khoshnood, M.R. Abedi, M. Ebrahimi, Fabrication a composite carbon paste electrodes (CPEs) modified with multi-wall carbon nano-tubes (MWCNTs/N, N-Bis (salicyliden)-1,3-propandiamine) for determination of lanthanum (III). *Eurasian Chem. Commun.* **3**, 627–634 (2021)
 39. Y. Shao, Y. Dong, L. Bin, L. Fan, L. Wang, X. Yuan, S. Zhao, Application of gold nanoparticles/polyaniline-multi-walled carbon nanotubes modified screen-printed carbon electrode for electrochemical sensing of zinc, lead, and copper. *Microchem J.* **170**, 106726 (2021)
 40. S. Tajik, H. Beitollahi, S. Shahsavari, F. Garkani-Nejad, Simultaneous and selective electrochemical sensing of methotrexate and folic acid in biological fluids and pharmaceutical samples using Fe₃O₄/ppy/Pd nanocomposite modified screen printed graphite electrode. *Chemosphere* **291**, 132736 (2021)
 41. M. Miraki, H. Karimi-Maleh, M.A. Taher, S. Cheraghi, F. Karimi, S. Agarwal, V.K. Gupta, Voltammetric amplified platform based on ionic liquid/NiO nanocomposite for determination of benserazide and levodopa. *J. Mol. Liq.* **278**, 672–676 (2019)

42. S. Tajik, Z. Dourandish, F. Garkani-Nejad, A. Aghaei Afshar, H. Beitollahi, Voltammetric determination of isoniazid in the presence of acetaminophen utilizing MoS₂-nanosheet-modified screen-printed electrode. *Micromachines* **13**, 369 (2022)
43. M. Coroş, S. Pruneanu, R.I. Stefan-van, Staden, Recent progress in the graphene-based electrochemical sensors and biosensors. *J. Electrochem. Soc.* **167**, 037528 (2019)
44. L. Fotouhi, M. Fatollahzadeh, M.M. Heravi, Electrochemical behavior and voltammetric determination of sulfaguanidine at a glassy carbon electrode modified with a multi-walled carbon nanotube. *Int. J. Electrochem. Sci.* **7**, 3919–3928 (2012)
45. J. Kremeskotter, R. Wilson, D.J. Schiffrin, B.J. Luff, J.S. Wilkinson, Detection of glucose via electrochemiluminescence in a thin-layer cell with a planar optical waveguide. *Meas. Sci. Technol.* **6**, 1325 (1995)
46. B. Fang, A. Gu, G. Wang, W. Wang, Y. Feng, C. Zhang, X. Zhang, Silver oxide nanowalls grown on Cu substrate as an enzymeless glucose sensor. *ACS Appl. Mater. Interfaces* **1**, 2829–2834 (2009)
47. M.B. Gholivand, L. Mohammadi-Behzad, Fabrication of a highly sensitive sumatriptan sensor based on ultrasonic-electrodeposition of Pt nanoparticles on the ZrO₂ nanoparticles modified carbon paste electrode. *J. Electroanal. Chem.* **712**, 33–39 (2014)
48. S. Felix, P. Kollu, S.K. Jeong, A.N. Grace, A novel CuO–N-doped graphene nanocomposite-based hybrid electrode for the electrochemical detection of glucose. *Appl. Phys. A* **123**, 1–9 (2017)
49. Y. Zhang, W. Lei, Q. Wu, X. Xia, Q. Hao, Amperometric nonenzymatic determination of glucose via a glassy carbon electrode modified with nickel hydroxide and N-doped reduced graphene oxide. *Microchim. Acta* **184**, 3103–3111 (2017)
50. G. Li, K. Li, A. Liu, P. Yang, Y. Du, M. Zhu, 3D flower-like β-MnO₂/reduced graphene oxide nanocomposites for catalytic ozonation of dichloroacetic acid. *Sci. Rep.* **7**, 1–7 (2017)
51. S. Kumar, V. Pandit, K. Bhattacharyya, V. Krishnan, Sunlight driven photocatalytic reduction of 4-nitrophenol on Pt decorated ZnO-RGO nanoheterostructures. *Mater. Chem. Phys.* **214**, 364–376 (2018)
52. P. Ni, Y. Sun, Y. Shi, H. Dai, J. Hu, Y. Wang, Z. Li, Facile fabrication of CuO nanowire modified Cu electrode for non-enzymatic glucose detection with enhanced sensitivity. *RSC Adv.* **4**, 28842–28847 (2014)
53. M.J. Song, S.W. Hwang, D. Whang, Non-enzymatic electrochemical CuO nanoflowers sensor for hydrogen peroxide detection. *Talanta* **80**, 1648–1652 (2010)
54. X. Gou, S. Sun, Q. Yang, P. Li, S. Liang, X. Zhang, Z. Yang, A very facile strategy for the synthesis of ultrathin CuO nanorods towards non-enzymatic glucose sensing. *New. J. Chem.* **42**, 6364–6369 (2018)
55. M.C. Buzzo, R.G. Evans, R.G. Compton, Non-haloaluminate room-temperature ionic liquids in electrochemistry: A review. *ChemPhysChem.* **5**, 1106–1120 (2004)
56. A. Abo-Hamad, M.A. AlSaadi, M. Hayyan, I. Juneidi, M.A. Hashim, Ionic liquid-carbon nanomaterial hybrids for electrochemical sensor applications: A review. *Electrochim. Acta* **193**, 321–343 (2016)
57. C. Yang, Y. Qing, K. An, Z. Zhang, L. Wang, C. Liu, Facile synthesis of the N-doped graphene/nickel oxide with enhanced electrochemical performance for rechargeable lithium-ion batteries. *Mater. Chem. Phys.* **195**, 149–156 (2017)
58. A.J. Bard, L.R. Faulkner, *Electrochemical Methods: Fundamentals and Applications* (Wiley, New York, 2001)
59. B.S. Jilani, C.D. Mruthyunjayachari, P. Malathesh, T.M. Sharankumar, K.V. Reddy, Electrochemical sensing based MWCNT-Cobalt tetra substituted sorbaamide phthalocyanine onto the glassy carbon electrode towards the determination of 2-Amino phenol: A voltammetric study. *Sens. Actuators B: Chem.* **301**, 127078 (2019)
60. S. Duan, X. Zhang, S. Xu, C. Zhou, Simultaneous determination of aminophenol isomers based on functionalized SBA-15 mesoporous silica modified carbon paste electrode. *Electrochim. Acta* **88**, 885–891 (2013)
61. X. Li, A. Zhong, S. Wei, X. Luo, Y. Liang, Q. Zhu, Polyelectrolyte functionalized gold nanoparticles-reduced graphene oxide nanohybrid for electrochemical determination of aminophenol isomers. *Electrochim. Acta* **164**, 203–210 (2015)
62. B. Kaur, R. Srivastava, Simultaneous electrochemical determination of nanomolar concentrations of aminophenol isomers using nanocrystalline zirconsilicate modified carbon paste electrode. *Electrochim. Acta* **141**, 61–71 (2014)
63. Z. Wang, H. Zhu, H. Zhang, G. Gao, Z. Sun, H. Liu, X. Zhao, Fabrication of the single-wall carbon nanotube compound polymer film electrode and the simultaneous electrochemical behavior of aminophenol isomers. *Electrochim. Acta* **54**, 7531–7535 (2009)

Publisher's Note Springer Nature remains neutral with regard to jurisdictional claims in published maps and institutional affiliations.

Springer Nature or its licensor holds exclusive rights to this article under a publishing agreement with the author(s) or other rightsholder(s); author self-archiving of the accepted manuscript version of this article is solely governed by the terms of such publishing agreement and applicable law.